Mid-Temperature Solid Oxide Fuel Cells with Thin Film ZrO_2 : Y_2O_3 Electrolyte

A. A. Solov'ev[a, z], **N. S. Sochugov**[a], **A. V. Shipilova**[a], **K. B. Efimova**[b], **and A. E. Tumashevskaya**[b]

[a]*Institute of High Current Electronics, Siberian Branch, Russian Academy of Sciences,*
prosp. Akademicheskii 2/3. Tomsk, 634055 Russia
[b]*Tomsk Polytechnic University, prosp. Lenina 30, Tomsk, 634050 Russia*
Received June 17, 2010

Abstract—Data on the mid-temperature solid-oxide fuel cells (SOFC) with thin-film ZrO_2–Y_2O_3 (YSZ) electrolyte are shown. Such a fuel cell comprises a carrying Ni–YSZ anode, a YSZ electrolyte 3–5 μm thick formed by vacuum ion-plasma methods, and a $LaSrMnO_3$ cathode. It is shown that the use of a combined method of YSZ electrolyte deposition, which involves the magnetron deposition of a 0.5–1.5-μm thick sublayer and its pulse electron-beam processing allows a dense nanostructured electrolyte film to be formed and the SOFC working temperature to be lowered down as the result of a decrease in both the solid electrolyte Ohmic conductivity and the Faradaic resistance to charge transfer. SOFC are studied by the methods of votammentry and impedance spectroscopy. The maximum power density of the SOFC under study is 250 and 600 mW/cm^{-2} at temperatures of 650 and 800°C, respectively.

Keywords: mid-temperature solid-oxide fuel cell, thin-film electrolyte, magnetron deposition, pulse electronic treatment, yttrium-stabilized zirconium dioxide, impedance spectroscopy

DOI: 10.1134/S1023193511040185

INTRODUCTION

Solid-oxide fuel cells (SOFC) represent attractive electrochemical generators that efficiently convert chemical energy of the hydrogen reaction with oxygen into electric energy with the minimum effect on the environment. However, the high working temperatures of SOFC (800–1000°C) give rise to two main problems typical of this type of fuel cells. First, to reach the working temperature, a SOFC should be heated at a low rate (slower than 300°C h^{-1}) to avoid destruction of ceramic parts of its structure due to the difference in their coeficients of thermal expansion (CTE). Second, the high temperatures were found to be responsible for the oxidation or corrosion of most of metals, the diffusion of electrode materials to the electrolyte to form nonconducting compounds, and the appearance of mechanical strains due to different CTE.

To be used in industry, the cost, the mechanical reliability, and electrochemical characteristics of SOFC must be improved, which can be achieved by lowering down the SOFC working temperature. This is why the active studies were aimed at decreasing the electrolyte resistance by changing Y_2O_3-stabilized ZrO_2 (YSZ) for other materials, e.g., cerium-doped samarium or gadolinium oxides that exhibited the higher ionic conductivity [1–3], or by decreasing the electrolyte thickness and thus minimizing the Ohmic losses [4].

So far, the majority of SOFC were fabricated based on tubular or planar fuel cells. A planar SOFC had a simpler design and its modification with a carrying anode made it possible to generate high power densities due to the low Ohmic resistance of the main substance [5]. The YSZ electrolytes were synthesized by different methods. For example, the methods of slip casting [6], screen printing [7], electrophoretic deposition [8], coating by dipping [9], and semidry pressing [10] were popular. However, the majority of mentioned methods failed to deposit micron layers. Methods conventionally used for the deposition of such YSZ films included high-frequency magnetron deposition, the sol-gel process, pulse laser evaporation, chemical gas-phase deposition, and dc magnetron deposition. In contrast to other methods, the magnetron deposition allowed the uniform and isotropic coatings to be obtained, was characterized by stability, provided independent control over the deposition parameters and the possibility of coating supports with high surface areas.

For SOFCs with the carrying anodes, the thin-film gas-impermeable electrolyte layer (1–3 μm thick) should be prepared on the surface of a porous support. For minimization of concentration losses, the support usually had the porosity of ca. 40% and the pore sizes from several hundred nanometers to ten micrometers.

[z] Corresponding author: andrewsol@mail.ru (A.A. Solov'ev).

Table 1. Characteristics of fuel cells with thin-film YSZ electrolyte

Fuel cell no.	Single-layer YSZ electrolyte thickness, µm	Double-layer YSZ electrolyte, µm		U_{nl}, mV at 650°C	P, mV cm^{-2} at 650°C
		sublayer	main layer		
1	3	–	–	0.75	60
2	5	–	–	0.85	60
3	9	–	–	–	–
4	–	0.35	2.5	0.92	155
5	–	1	2.5	1.02	125
6	–	1.5	2.5	1.03	210
7	–	2	2.5	1.02	250

Hence, it is evident that to obtain a highly gas-permeable ZrO_2–Y_2O_3 (YSZ) layer, the porous SOFC anodes should be subjected either to surface modification aimed at the development of modified and interfacial layers on their surfaces or at the modification of the thin YSZ layer in order to increase its gas-proof properties [11–13].

In the present publication, we considered the characteristics of a mid-temperature SOFC operating at temperatures below 800°C, which comprised a cermet Ni/YSZ anode, an YDZ electrolyte deposited by magnetron sputtering, and a "spread" $LaSrMnO_3$ cathode. An important feature of our method of SOFC preparation was the use of pulse electron-beam treatment in the intermediate stage of electrolyte deposition. As the result of such treatment, the irradiated layers acquired the nanograin structure with unique properties [14, 15]. SOFC Units were studied in the temperature range from 600 to 800°C by voltammetric and impedance spectroscopic methods. Scanning electron microscopic investigations were performed with the aim of studying the effect of the electron-beam treatment on the structure and morphology of the YSZ electrolyte surface. The dependence of electrochemical characteristics of fuel cells on the conditions of deposition of electrolyte layers, the temperature, and the consumption of working gases was analyzed.

EXPERIMENTAL

Preparation of Fuel Cells

The initial material for porous anodes represented a mixture of nickel oxide with yttrium-stabilized zirconium oxide shaped as a ribbon. The latter was manufactured by ESL ElectroScience (USA) by a method of slip casting; the suspension used included powders of nickel oxide and YSZ, a thermoplastic binder, and a surface-active substance. Prior to high-temperature sintering, the anode samples were 24 mm in diameter

and ca. 550 µm thick. Sintering of NiÎ/YSZ samples was conducted in air atmosphere, at temperature of 1450°C and with 2-h isothermal exposure. After sintering, the sample diameter decreased to 20 mm. Anodic supports represented double layer structures which consisted of the main (0.5 mm thick, pore diameter 1.5–2 µm) and the functional (15 µm thick, pore size ~0.6 µm) layers. The functional layer adjacent to electrolyte acted as the electrochemically active layer and consisted of small Ni and YSZ grains in order to increase the interface and decrease the polarization losses. The main layer served as the current-collecting and gas-distributing layer and for this purpose had the pore size sufficient for the delivery of fuel to the electrolyte and the removal of reaction products. The gas-permeability (G) of this double-layer anode was ~6.3 × 10^{-5} mol m^{-2} s Pa.

The cathode was formed by spreading and drying the $La_{0.80}Sr_{0.20}MnO_{3-x}$ paste manufactured by Nex-Tech Materials, Ltd. (USA). Broadly speaking, $La_xSr_{1-x}MnO_3$ (LSM) was the most popular material in the production of SOFC due to its good compatibility with YSZ.

Table 1 shows all fuel cells under study that had similar anodes and cathodes and differed only in the electrolyte thickness and deposition methods. To apply a single-layer thin-film electrolyte on samples 1, 2, and 3, we used a method of pulse reactive magnetron sputtering of a $Zr_{0.86}Y_{0.14}$ cathode. The thickness of electrolyte layers of these samples was 3, 5, and 9 µm, respectively. The YSZ electrolyte was applied in the Ar/O_2 atmosphere at a pressure of 0.2–0.3 Pa on supports heated to 600°C. The magnetron operated in the pulsed mode with the frequency of 50 kHz and the discharge power of 1.5 kW. The deposition rate of the YSZ film was 2.5 µm h^{-1}.

Fuel cells 4–7 were prepared with the double-layer electrolyte. In the first stage, a YSZ sublayer with the thickness of 0.35, 1, 1.5, and 2 µm, respectively, was
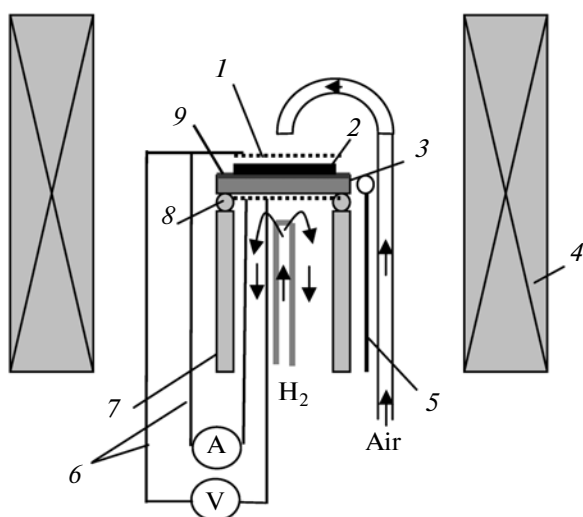
Fig. 1. Illustration of a unit used for measuring electrochemical characteristics of SOFC: (*1*) Pt gauze, (*2*) cathode, (*3*) anode, (*4*) furnace, (*5*) thermocouple, (*6*) Pt wires, (*7*) an Al_2O_3 tube for fixing the fuel cell, (*8*) sealing, (*9*) electrolyte.

applied on the porous anode. Then the samples were subjected to the pulse electron beam processing with the following characteristics: electron energy $E_e = 10{-}12$ keV, beam current ~15 kA, beam energy density $E_s = 0.8$ J/cm^2, pulse length 2.5 μs, number of effective pulses $N = 2{-}3$. The melt quenching rate reached ~10^{10} K s^{-1} on the surface. The working pressure in the chamber was at a level of 5.07×10^{-6} Pa. After the electron-beam processing (EBP), the second electrolyte layer with a thickness of ~2.5 μm was deposited and then the LaSrMnO$_3$ cathode was applied. The cathode was dried at a temperature of 125°C and its sintering occurred only in the course of fuel cell testing at working temperatures of 600–800°C. The experiments on the EBP of porous anodes and the YSZ sublayer were described in more detail in [16].

Fuel Cell Tests

Figure 1 illustrates the ProboStat^{TM} (NorECs, Norway) unit for studying the characteristics of individual SOFCs. The studied cell was fixed on a tube of aluminum oxide with the diameter of 20 mm; a sealing glass ring was used for its sealing. Platinum gauzes with the diameter of 15 mm were used as both anodic and cathodic current collectors. Each collector was connected with a platinum wire; these wires were used for measuring the current and the voltage. The sample was heated to the working temperature at a rate of 300 deg h^{-1}. Wetted hydrogen and air (oxygen) were supplied to a fuel cell at the rates of 20–80 ml min^{-1} and 50–250 ml min^{-1}, respectively. The fuel cell characteristics were studied by voltammetric and impedance spectroscopic methods using the following instruments: P-150S potentiostat

and Z-500P impedancemeter (Elins, Russia). The impedance was measured in the frequency range of $0.2{-}5 \times 10^5$ Hz and the ac signal amplitude of 10 mV under open circuit conditions and under a load. The obtained impedance spectra were analyzed using the Z-View 2.3f program (Scribner Associates Inc., USA) by the method of equivalent circuits.

Studies of Sample Microstructure

After studying the electrochemical characteristics, the fuel cells were analyzed by a scanning electron microscope Philips SEM 515. The real thicknesses of fuel cell components were also measured by electron microscopy.

Gas-Permeability Measurements

The gas permeability of electrolyte layers with respect to nitrogen was studied on a home-made setup, which represented two hermetically sealed compartments divided by the sample under study. Each compartment was equipped with gas-delivery tubes through which the head compartment was filled with nitrogen and the working compartment was freed from the gas that diffused into it. The amount of nitrogen passed through the sample was measured by the volumetric method (by measuring the volume of gas passed at a constant pressure). The gas that diffused through the sample entered a capillary of a constant cross section and the amount of gas flowed in time was assessed by the travel of a liquid drop in the capillary.

RESULTS AND DISCUSSION

Microstructure of Fuel Cells with Thin Film YSZ Electrolyte

Figure 2 shows the cross sections of the anode/single-layer electrolyte and anode/double-layer electrolyte structures and also the electrolyte surface. Apparently, the YSZ coatings applied by magnetron deposition on a porous support had the columnar structure (Fig. 2a). However, the films were sufficiently dense and demonstrated good adhesion to the anode. The gas permeability of sample 2 with the thickness of 5 μm amounted to 2.1×10^{-7} mol m^{-2} s^{-1} Pa^{-1}, which was 300 times lower as compared with the original anodic support (6.25×10^{-5} mol m^{-2} s^{-1} Pa^{-1}).

Figure 2b shows the cross section of sample 6 with the double-layer electrolyte the formation of which started with the deposition of 1.5 μm thick YSZ sublayer followed by electron-beam processing. As the result, the sublayer was recrystallized due to the high-rate heating and cooling, the columnar electrolyte structure transformed into a denser structure, which was also accompanied by surface smoothing. Hence, the growth and the formation of the second electrolyte layer on the processed sublayer started on the smooth surface of the latter rather than on the vertexes of Ni
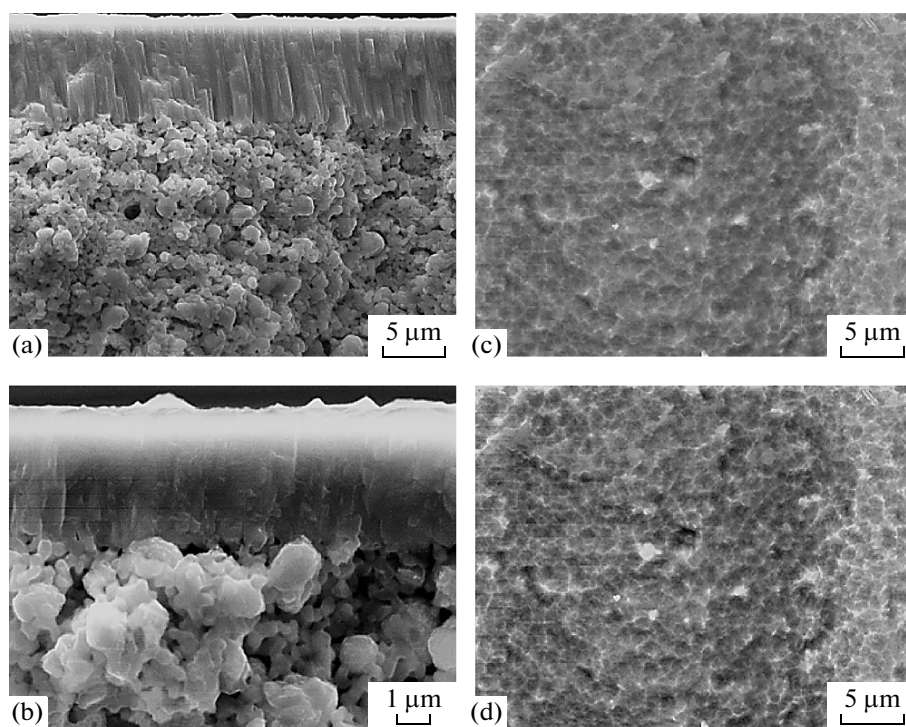
Fig. 2. Cross sections of samples with the following structures: (a) Ni-YSZ/single-layer YSZ electrolyte, (b) Ni-YSZ/double-layer YSZ electrolyte, (c, d) surfaces of (c) single- and (d) double-layer YSZ electrolytes.

and YSZ grains in the porous anode that would inevitably favor the formation of pores in the coating. The surface state is known to play an important role in the initial stage of coating formation and largely determine the future structure. As the result, the second electrolyte layer had the pore-free structure of the processed sublayer and the boundary between two layers was absolutely indistinguishable. The gas-permeability of the double-layer electrolyte prepared using the electron-beam processing was twice lower as compared with the single-layer electrolyte of the same thickness and equal to 1.01×10^{-7} mol m^{-2} s^{-1} Pa^{-1}.
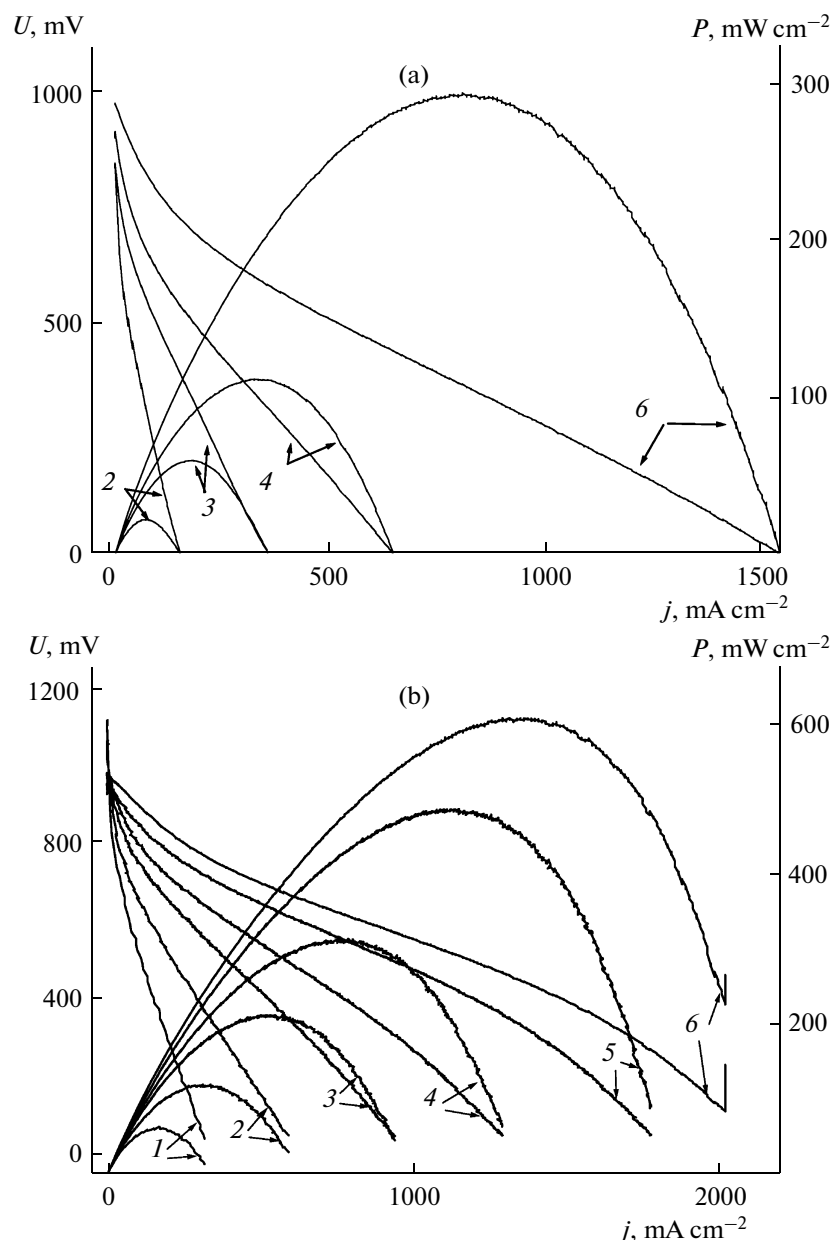
Voltammetric Characteristics of Fuel Cells with Thin Film YSZ Electrolyte

Figure 3 show voltammetric and power characteristics of samples with single-layer (fuel cell 2) and double-layer (fuel cell 6) electrolytes. The no-load voltage U_{nl} of these samples at temperatures of 600–800°C was equal to 840–960 and 950–1060 mV, respectively. The U_{nl} values of samples with double-layer electrolyte approached those theoretically possible in air (1080 mV). This pointed to the lower gas-permeability of the double-layer electrolyte, which correlated with both the directly assessed permeability and the electrolyte structure observed by an electron microscope.

Voltammetric characteristics (VAC) of both cells shown in Fig. 3 are nonlinear. The first "fast" VAC region (from 0 to 40–400 mA, depending on the temperature) was associated with the activation losses due to the energy consumption in several processes. The latter involved the gas-phase diffusion of reagents to electrodes, the adsorption, the dissociation and the ionization, the surface diffusion to electrochemically active centers, and the penetration of ions into electrolyte and electrodes.

At high current densities (above 1 mA cm^{-2}), in fuel cell 6, the voltage drop accelerated due to the appearance of concentration losses. This kind of polarization was associated with the fact that the concentration of species in the reaction zone through which a current flowed differed from the concentration of reagents in the anode bulk, because the delivery and the removal of substances lagged behind their consumption on the electrode.

At a temperature of 800°C, the power densities generated by fuel cells 2 and 6 differed more than two-fold being 300 and 600 mW/cm^{-2}, respectively, at the potential of 400 mV. As the temperature lowered down to 600°C, the difference between power densities of these cells increased to four-fold. Apparently, this is due to the smaller resistance of the double-layer electrolyte, which testifies that EBP combined with magnetron deposition holds much promise in the manufacturing mid-temperature SOFC.

Fig. 3. Voltammetric and power characteristics of fuel cells (a) 2 and (b) 6 at different temperatures, °C: (*1*) 550, (*2*) 600, (*3*) 650, (*4*) 700, (*5*) 750, (*6*) 800. H_2: 40 ml min^{-1}; air: 150 ml min^{-1}.

Impedance Spectroscopy of Fuel Cells with Thin Layer YGZ Electrolyte

Figure 4 shows impedance spectra of cells 2 and 4 measured in the no-load mode at temperatures of 600, 650, and 700°C. They are described by two partly overlapping semicircles with small radii at high frequencies and large radii at low frequencies. The high-frequency semicircle was poorly discernible but became more pronounced as the temperature decreased. According to the general theory of electrochemical impedancemetry, the intersection point of the high-frequency hodograph region with the impedance real axis corresponded to the Ohmic resistance of a fuel cell (R_E), which included the resistances of the electrolyte, two electrodes, current collectors, and connecting wires. The intersection point of the low-frequency hodograph region with the impedance real axis determined the total resistance of a fuel cell ($R_E + R_p$) comprising the Ohmic resistance of the cell, its resistance associated with concentration polarization (mass transfer resistance), the polarization resistance caused by the charge transfer $\left(R_{ct}^{eff} \right)$, and other types of polarization resistance induced by, e.g., adsorption processes, etc. Thus, the total polarization resistance of
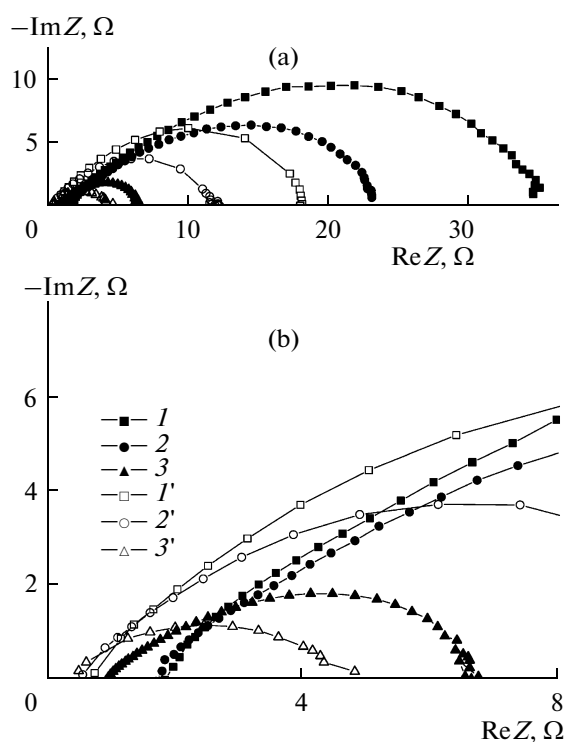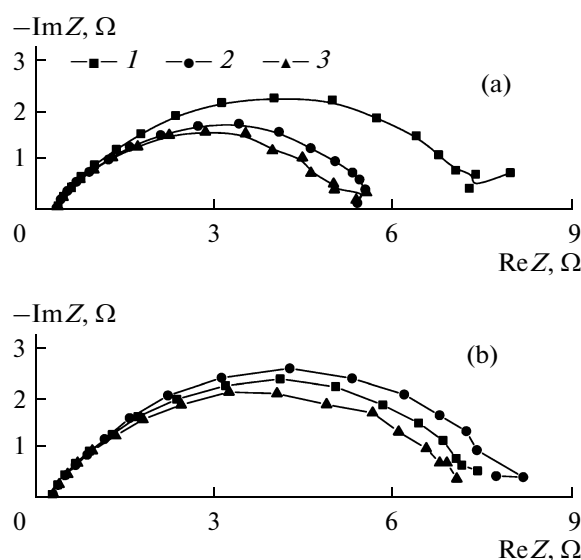
Fig. 4. (à) Impedance spectra of fuel cells (*1–3*) 2 and (*1'–3'*) 4 recorded at temperatures, °C: (*1, 1'*) 600; (*2, 2'*) 650; (*3, 3'*) 700. (b) Enlarged high-frequency region of these impedance spectra. H_2: 40 ml min^{-1}; air: 150 ml min^{-1}.

Fig. 5. Impedance spectra of fuel cell 4 at 650°C and different consumption rates of (a) hydrogen and (b) oxygen. Hydrogen consumption, ml min^{-1}: (*1*) 20, (*2*) 40, (*3*) 80 (air consumption 250 ml min^{-1}); oxygen consumption, ml min^{-1}: (*1*) 50, (*2*) 150, (*3*) 250 (hydrogen consumption rate 40 ml min^{-1}).

electrodes (R_p) could be determined from the impedance spectra as well.

For fuel cell 2, the Ohmic resistance increased from 0.25 to 1.8 Ω as the temperature decreased from 800 to 600°C. For fuel cells 4, 6, and 7, as the temperature decreased in the same temperature range, R_E increased from 0.27 to 0.92, 0.42, and 0.31 Ω, respectively. Thus for 800°C, the Ohmic resistance of samples under study was approximately unchainged and equal to 0.25–0.27 Ω but, as the temperature increased, the samples with double-layer electrolytes had substantially lower Ohmic resistances. Moreover, the difference between R_E of fuel cells with single- and double-layer electrolytes increased with a decrease in the temperature. Insofar as the obtained samples differed only in the methods preparation while the electrolyte thicknesses and the Ohmic resistances of electrodes, current collectors, and connecting wires were the same for all cells, the changes in R_E were directly associated with the changes in the conductivity of the YSZ electrolyte. The lower resistance of an electrolyte subjected to EBP was explained by the fact that the pulse fusion was capable to form layers with the ultrafine-grain and nanocrystalline structure [17].

According to Fig. 4, fuel cell 4 with the double-layer electrolyte exhibited not only the lower Ohmic resistance as compared with a cell with single-layer electrolyte but also the smaller polarization resistance

R_p. For samples 4–7, the polarization resistance was in the range of 10–16 Ω, whereas for fuel cell 2, this value was equal to 22 Ω. This means that the EBP affected not only the properties of the YSZ sublayer but also changed the surface of the contact between the Ni/YSZ anode and the YSZ electrolyte. This could increase the three-phase boundary between the anode and the electrolyte and decrease the polarization resistance associated with the charge transfer.

Figure 5 illustrates the effect of gas consumption on the impedance spectra of fuel cell 4. The measurements were performed in the no-load mode. It is evident that in the high-frequency range, the hydrogen and oxygen consumption had no effect on the cell impedance, whereas in the low-frequency range, the impedance decreased with the increase in gas consumption. Voltammetric and power characteristics indicated that for different gas consumption rates at low current densities, the cell potential remained unchanged. However, for a high current density, the gas consumption had a considerable effect on the VAC. This suggested that the characteristics of a fuel cell were largely limited by the mass transport and the electrochemical reaction at the interface. As the gas consumption decreased, the maximum power density decreased. The power density decreased from 170 to 150 mW cm^{-2} as the hydrogen consumption decreased from 80 to 20 ml min^{-1} and from 240 to 225 mW cm^{-2} as the oxygen consumption dropped from 250 to 50 ml min^{-1}.

As was already noted above, the impedance of a cell with the thin-film YSZ electrolyte in the no-load mode
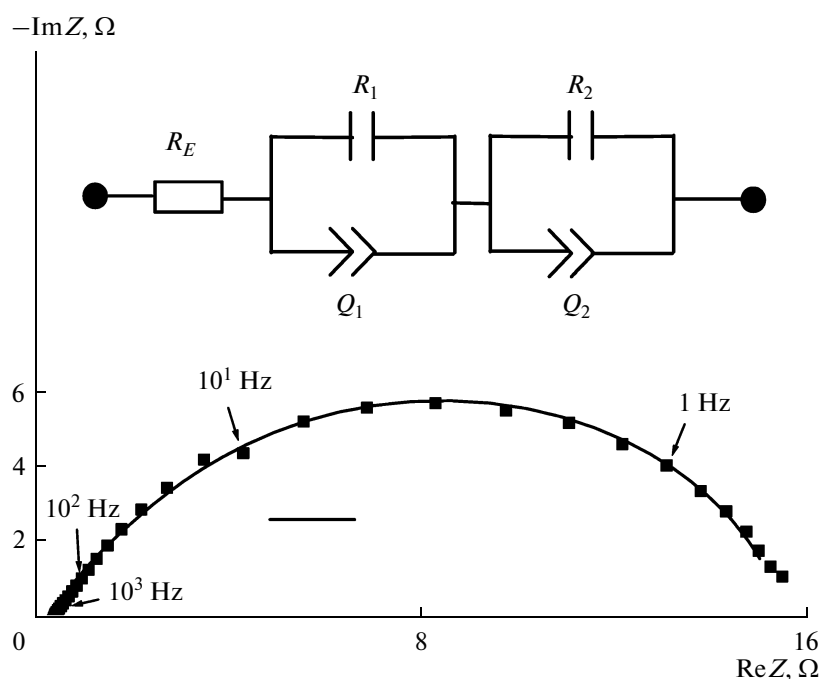
Fig. 6. Impedance spectra of fuel cell 7: calculated (curve) and measured (points) at 650°C and also the equivalent circuit of fuel cell. H_2: 40 ml min^{-1}; air: 150 ml min^{-1}.

was characterized by the presence of large-circle arcs at low frequencies and small-circle arcs at high frequencies. Under a load, the cell impedance had a similar form. This suggested that at least two different electrode processes could be responsible for the high- and low-frequency arcs. The similar impedance spectra were observed [18] for SOFC that comprised a carrying anode, an YSZ electrolyte, and a LSM-YSZ/LSM double-layer cathode.

The impedance spectrum of fuel cell 7 was modeled by an equivalent circuit shown in Fig. 6, where R_E is the total Ohmic resistance, (R_1, Q_1) and (R_2, Q_2) pertain to the high- and low-frequency arcs, respectively. The equivalent circuit included two series circuits each containing a resistance and a constant phase element (CPE) connected in parallel.

The CPE was often used in equivalent circuits for modeling the impedance and expressed as $Q = A^{-1}(j\omega)^{-n}$, where A is the pseudocapacitance, F cm^{-2} s^n; ω is the angular rate, rad s^{-1}; $j = (-1)^{1/2}$; and n is the power index of CPE. For $n = 1$, the constant phase element represented a pure capacitance; for $n = 0$, CPE was a resistance, and at $n = 0.5$, CPE transformed into the Warburg element and modeled the diffusion of reagents. The presence of a CPE in the equivalent circuit could point to the reactivity distributed over the surface, the surface heterogeneity, roughness, or fractal geometry, the electrode porosity, the current and potential distribution according to the electrode geometry [19].

In the Z-View program we used for analyzing the impedance, the constant phase element was given by two parameters designated as CPE-T and CPE-P. The CPE-T parameter corresponded to pseudocapacitance A and CPE-P was identified with the power index n in Eq. (1) that characterized the geometric properties of the surface [20].

Resistances R_E, R_1, R_2 and constant phase elements Q_1, Q_2 for fuel cell 7 were calculated based on impedance spectra measured in the no-load mode at different temperatures (Table 2).

At 800°C , the Ohmic resistance of fuel cells with double-layer electrolyte was ~0.23 Ω cm^2. Based on the YSZ conductivity equal to ~0.04 S cm^{-1} at 800°C (the Ohmic resistance of the YSZ electrolyte with the thickness of 10 μm ~0.025 Ω cm^2) [21], the Ohmic resistance of the YSZ electrolyte 3–5 μm thick should be ~0.008–0.012 Ω cm^2. The difference observed in practice was probably due to the additional contact resistance at the LSM/YSZ interface, because, in our case, the LSM cathode was not sintered at temperatures commonly used in practice (1100–1250°C) and also due to the resistance at the electrode boundary with current collectors.

As the working temperature increased, the polarization resistances R_1 and R_2 and also the time constants R_1Q_1 and R_2Q_2 corresponding to high- and low-frequency arcs considerably decreased. For instance, R_1 and R_2 at temperature 750°C were equal to 0.67 and 2.14 Ω, which was 2- and 6-fold lower than their corresponding values at 650°C. The time constants R_1Q_1

Table 2. Parameters calculated using the Z-View 2.3f program for impedance spectra of fuel cell 7 measured in the no-load mode at different temperatures

t, °C	R_E, Ω	High-frequency arc			Low-frequency arc		
		R_1, Ω	Q_1, F s^n	R_1Q_1 (τ_B, ms)	R_2, Ω	Q_2, F s^n	R_2Q_2 (τ_H, ms)
650	0.30	1.6	$A = 0.14$ $n = 0.77$	224	13.6	$A = 0.1$ $n = 0.87$	1360
700	0.29	1.2	$A = 0.12$ $n = 0.69$	144	5.3	$A = 0.05$ $n = 0.79$	265
750	0.28	0.67	$A = 0.023$ $n = 0.69$	15.4	2.14	$A = 0.006$ $n = 0.75$	12.8
800	0.27	–	–	–	1.29	$A = 0.005$ $n = 0.75$	6.5

and R_2Q_2 also substantially decreased as the temperature lowered from 650 to 750°C , i.e., by the factors of 15 and over 100, respectively. For 800°C , the small-circle arc corresponding to the high-frequency spectral range disappeared altogether and the impedance was modeled by a single circuit comprising a resistance and a CPE connected in parallel.

The power index n fitted a range from 0.7 to 0.9 in both the high- and low-frequency regions (Table 2). Its values were close to those obtained in a study [22] devoted to the kinetics of the electrochemical reaction at the LSM/YSZ interface. The power index n for cathodes sintered at different temperatures changed from 0.5 to 0.8. However, it remained unclear why n increased with the increase in the temperature; the analogous dependence was mentioned in the literature [18, 22].

Insofar as the contribution of the anodic polarization to the overall losses in a fuel cell was far below the cathodic contribution, the electrode polarization in a SOFC was assumed to be mainly cathodic [22]. In [24], the impedance spectra measured for a SOFC with the composite LSM-YSZ cathode was also approximated by two semicircles. The first semicircle pertaining to the high-frequency spectrum part corresponded to the transfer of oxygen ions from the electrode to the electrolyte. The second located in the low-frequency zone corresponded to the dissociative adsorption of oxygen and/or its surface diffusion.

The decrease in the voltage on a fuel cell upon imposing a load was accompanied by a decrease of polarization resistances R_1 and R_2 and also of the time constants R_1Q_1 and R_2Q_2. This suggested that the processes of oxygen ion transfer and the surface dissociation with diffusion were activated with the application of an electric load [18].

The obtained results demonstrated that the proposed method of formation of a thin-film electrolyte allowed fabricating SOFC with sufficiently high specific characteristics at moderate (650°C) temperatures and also that the further improvement of the SOFC characteristics should be directed at the elimination of the polarization resistance, especially, of the cathode. We are planning to use a composite LSM-YSZ cathode for this purpose, because the use of composite cathodes allows the three-phase boundary between the cathode and the electrolyte to be substantially increased thus decreasing the polarization resistance to the charge transfer.

CONCLUSIONS

In this study, we demonstrated that the methods of magnetron deposition and electron-beam processing showed promise in the formation of a thin-film electrolyte for mid-temperature solid-oxide fuel cells. The maximum power density of fuel cells prepared by the aforementioned methods was 200–250 mW cm^{-2} at 650°C. This several times exceeded the power densities typical of fuel cells with the carrying electrolyte under the given conditions and was achieved due to both the decrease in the YSZ electrolyte thickness and resistance and the optimization of its structure. The functional characteristics of the developed mid-temperature SOFC can be substantially improved by lowering down the cathodic polarization and decreasing the contact resistances at the cathode/electrolyte and electrode/current collector interfaces.

REFERENCES

1. Doshi, R., Richards, V.L., Carter, J.D., Wang, X.P., and Krumpelt, M., *J. Electrochem. Soc.*, 1999, vol. 146, p. 1273.

2. Xia, C.R. and Liu, M.L., *Solid State Ionics*, 2001, vol. 144, p. 249.

3. Xia, C.R., Chen, F.L., and Liu, M.L., *Electrochem. Solid-State Lett.*, 2001, vol. 4, p. 52.

4. De Souza, S., Visco, S.J., and De Jonghe, L.C., *Solid State Ionics*, 1997, vol. 98, p. 57.

5. Zhao, F. and Virkar, A.V., *J. Power Sources*, 2005, vol. 141, p. 79.

6. Nguyen, T.L., Honda, T., Kato, T., Iimura, Y., Kato, K., Negishi, A., Nozaki, K., Shiono, M., Kobayashi, A., Hosoda, K., Cai, Z.F., and Dokiya, M., *J. Electrochem. Soc.*, 2004, vol. 151, no. 8, p. 1230.

7. Rotureau, D., Viricelle, J.-P., Pijolat, C., Caillol, N., and Pijolat, M., *J. Eur. Ceram. Soc.*, 2005, vol. 25, p. 2633.

8. Sarkar, P., Yamarte, L., Rho, H.S., and Johanson, L., *Int. J. Appl. Ceram. Technol.*, 2007, vol. 4, no. 2, p. 103.

9. Zhang, L., Quan, HeH., Kwek, W.R., Ma, J., Tang, E.H., and Jiang, S.P., *J. Am. Ceram. Soc.*, 2009, vol. 92, no. 2, p. 302.

10. Rifau, A., Zainal, Z., Mutharasu, D., Fauzi, A., Kiros, Y., Zhu, B., and Zanzi, R., *Am. J. Appl. Sci*, 2006, vol. 3, no. 9, p. 2020.

11. Wanzenberg, E., Tietz, F., Panjan, P., and Stover, B., *Solid State Ionics*, 2003, vol. 159, p. 1.

12. Vervoort, A.G.J., Scanlon, P.J., Ridder, M., Brongersma, H.H., and Welzenis, R.G., *Nucl. Instrum. Methods Phys. Res., Sect. B*, 2002, vol. 190, p. 813.

13. Hobein, B., Tietz, F., Stover, D., Cekada, M., and Panjan, P., *J. Eur. Ceram. Soc.*, 2001, vol. 21, p. 1843.

14. Rotshtein, V.P., Ivanov, Yu.F., Proskurovsky, D.I., Karlik, K.V., Shulepov, I.A., and Markov, A.B., *Surf. Coat. Technol*, 2004, vol. 180-181, p. 382.

15. Ozur, G.E., Proskurovsky, D.I., Rotshtein, V.P., and Markov, A.B., *Laser Part. Beams*, 2003, vol. 21, p. 157.

16. Soloviev, A.A., Sochugov, N.S., Shipilova, A.V., Rotshtein, V.P., and Kovsharov, N.F., *Int. J. Alternative Energy Ecol.*, 2009, vol. 9, no. 77, p. 27.

17. Rotshtein, V, Ivanov, Yu, and Markov, A, in *Materials Surface Processing by Directed Energy Techniques*, Pauleau, Y., Ed., Amsterdam: Elsevier, 2006, ch. 6, p. 205.

18. Leng, Y.J., Chan, S.H., Khor, K.A., and Jiang, S.P., *Int. J. Hydrogen Energy*, 2004, vol. 29, p. 1025.

19. Jorcin, J.B., Orazem, M.E., Pebere, N., and Tribollet, B., *Electrochim. Acta*, 2006, vol. 51, p. 1473.

20. Lopez, D.A., Simison, S.N., and De Sanchez, S.R., *Electrochim. Acta*, 2003, vol. 48, p. 845.

21. De Souza, S., Visco, S.J., and De Jonghe, L.C., *J. Electrochem. Soc.*, 1997, vol. 144, no. 3, p. 35.

22. Heuveln, F., Characterization of Porous Cathodes for Application in Solid Oxide Fuel Cells, *Thesis*, Netherlands: University of Twente, 1997, p. 189.

23. Macdonald, J.R., *Solid State Ionics*, 1984, vol. 13, p. 147.

24. Kim, J.D., Kim, G.D., Moon, J.W., Park, Y.I., Lee, W.H., Kobayashi, K., Nagai, M., and Kim, C.E., *Solid State Ionics*, 2001, vol. 143, p. 379.

SPELL: 1. ok